Surface settlement behavior due to various active trapdoors forms in granular soils

N. Farasat, T. Newson

Civil Engineering, Western University, London, Canada, nfarasat@uwo.ca, tnewson2@uwo.ca

ABSTRACT: Trapdoor models serve as analog systems to study soil–structure interaction in underground structures such as tunnels and pipelines. They replicate ground load redistribution when support elements yield, providing insights into arching and settlement mechanisms. This study investigates surface and sub-surface settlement behavior of active trapdoors under 60g in centrifuge experiments with dry sand with further investigation through numerical simulations. Physical models using medium sand with varying relative densities (D_r = 30–90%) were tested. Additional tests examined modified trapdoor geometries using a flexible membrane and a rigid half-tunnel shape. Soil displacements were tracked using GeoPIV. Supporting finite element analyses employed a porous elastic cap plasticity model to simulate soil behavior. Results showed that increasing relative density led to shallower and narrower settlement troughs. A flexible boundary (membrane) configuration reduced surface deformation by redistributing stresses more evenly, whereas a half-tunnel circular shape produced sharper move, localized settlements due to stronger arching. Overall, the flexible boundary promoted smoother stress redistribution, while the half-tunnel showed intermediate behavior between the flexible and the traditional rigid trapdoor conditions. These findings demonstrate how density, and boundary flexibility and shape influence surface settlements during trapdoor actuation, providing practical insights for tunnel, pipeline, and trench model design in granular soils.

1 INTRODUCTION

The trapdoor problem has long been regarded as a benchmark in geotechnical engineering for investigating soil arching phenomena and stress redistribution around buried structures, such as tunnels, foundations and anchor plates (Bosscher & Gray, 1986; Handy, 1985; Ladanyi & Hoyaux, 1969; McNulty, 1965; Terzaghi, 1943; Wang & Yen, 1974). Originating from Terzaghi (1943) early observations of arching in retaining walls and trapdoors, this configuration offered a controlled setting to observe how soil transfers load away from a yielding boundary and mobilizes shear resistance along adjacent rigid zones. Both experimental and numerical models have since developed this concept, providing valuable insights into pre- and post-failure mechanisms, arching efficiency, and soil reaction curves under active (downward) trapdoor displacement (Bosscher and Gray 1986; Ladanyi and Hoyaux 1969; McNulty 1965). Early studies revealed characteristic features such as stress concentrations along trapdoor edges, settlement trough formation at the soil surface, and the progressive development of slip lines and shear bands with increasing downward displacements (Handy, 1985; Terzaghi, 1943; Wang & Yen, 1974). While these models captured important aspects of soil–structure interaction, they were generally constrained by their simplifying assumptions, including rigid trapdoor boundaries, uniform soil layers, and fully drained or dry soil conditions. Such idealizations, while useful for analytical clarity, these overlook more realistic field cases where soils are partially saturated, boundary elements may deform or rotate, and trapdoor geometries more closely resemble tunnel linings and other underground structures rather than flat plates (McNulty, 1965)

Recent numerical efforts (e.g. Osman, Jacobsz, and Purchase 2019) used advanced methods like the Coupled Eulerian–Lagrangian (CEL) formulation to model shear band evolution and cavity propagation in deep trapdoor settings. These studies emphasized the role of relative density (D_r) and dilation angle (ψ) in defining the failure surface trajectory, but did not explore varying moisture conditions, nor did they simulate tunnel-like geometries. Similarly, George and Dasaka (2021) employed the Hardening Soil model to classify active and passive arching zones and identify critical principal stress orientations. While effective in delineating zones of influence, these models assumed planar soil surfaces and uniform dry materials, limiting their applicability to field-scale underground construction problems where density and structural flexibility are key.

The compressive nature of soil arches and their residual loading mechanisms have been discussed in depth by George and Dasaka (2023), who derived polynomial-based arch shapes using centrifuge data and Mohr-circle interpretations. Yet, the assumed symmetry and rigidity of the boundary conditions in those studies still left the effects of trapdoor curvature and compressibility unexplored. Recent analytical and limit analysis approaches (Rai & Chavda, 2023) extended the assessment to sloped grounds and cohesive-frictional soils, but again under fully drained or idealized dry conditions.

However, implications for tunnel-like geometries and flexible boundaries remain insufficiently quantified. Recent works have begun addressing these aspects: e.g. numerical analyses of multi-span systems with viscoelastic supports (Al-Naddaf & Han, 2021) which captures more realistic stress redistribution and experimental studies on buried flexible pipes under localized ground loss (Costa et al., 2009) which shows boundary flexibility modifies the shape of settlement troughs and stress paths. The present study investigates trapdoor-induced arching in dry sand with centrifuge experiments and numerical simulations, examining influences of rigid and flexible trapdoors. These advance understanding of soil-structure interaction for deformable boundaries relevant to tunnel-like geometries.

2 EXPERIMENTAL METHODOLOGY

2.1 Overview

A series of centrifuge-based active trapdoor experiments was conducted at 60 g to investigate soil arching and settlement behavior in dry sand. The experimental program systematically varied relative density and trapdoor boundary conditions to isolate their effects on stress redistribution and deformation. Three configurations were examined: a) a rigid flat trapdoor, b) a rigid half-circular trapdoor, and c) a flexible membrane-supported trapdoor. Trapdoor movements were applied under displacement control (at a fixed rate of 5 mm/s), and soil deformation was captured using Particle Image Velocimetry.

2.2 Materials

The material used was Barco 32 silica sand, a medium, sub-rounded to angular material with a mean grain size of 0.35 mm. This has been characterized previously based on shear strength parameters, particle size distribution, and peak friction angle (Deljoui & Newson, 2012) [see Figures Figure 1 to Figure 3]. The bulk density (ρ) of the dry sand varied between 1405 and 1691 kg/m³, corresponding to the loosest and densest packing conditions, respectively (Deljoui & Newson, 2012). Oedometer curves for a density of 1600 kg/m^3 are also shown in Figure 4.

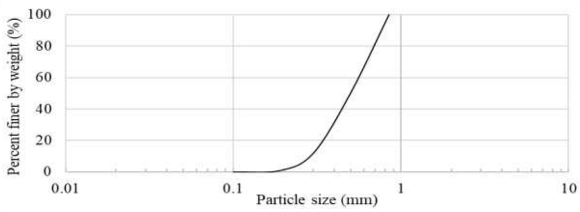

Figure 1. Soil particle distribution for Barco 32 sand

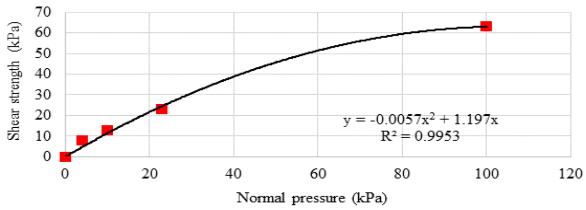

Figure 2. Direct shear tests results for Barco 32 sand with peak nonlinear failure envelope (Deljoui & Newson, 2012)

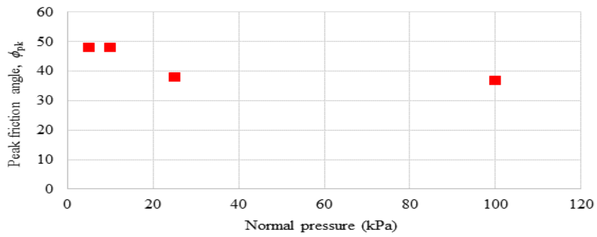

Figure 3. Peak friction angle against normal pressure

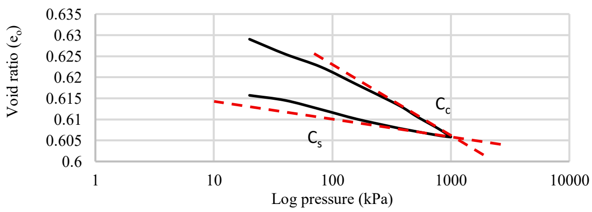

Figure 4. Oedometer curves for D_r of 1600 kg/m^3

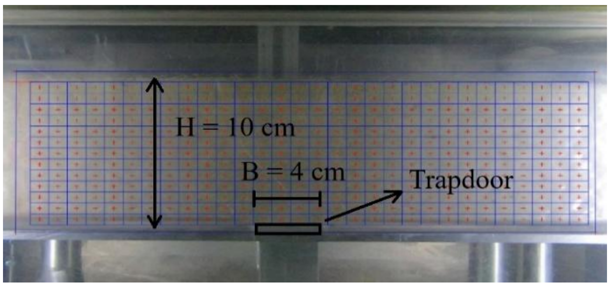

Figure 5. Experimental trapdoor model with PIV grid

2.3 Centrifuge modeling

2.3.1 Trapdoor models

The plane strain centrifuge model container had internal dimensions of 0.48 m × 0.15 m × 0.075 m, and Barco sand was placed to a height of 0.1 m (0.48 m × 0.10 m × 0.075 m), representing the soil domain above the trapdoor (see Figure 5) and placed in the Western university drum centrifuge. Table 1 summarizes the soil tests investigated in this study, covering tests with variations in relative density (D_r), density, cohesion, and boundary type (membrane and rigid half-circle) to capture a wide range of soil responses. The trapdoor width (B) is 0.04 m, and two more boundary configurations were tested, including a flexible membrane trapdoor (Test #7) and a rigid half-circle trapdoor (Test #8), as shown in Figure 6. The membrane was made of a 3 mm-thick latex sheet with a total length of 0.12 m (3B), while the rigid half-circle had a diameter of 0.04 m. The free length of the flexible membrane spans the rigid opening width B, while the extended lengths of 1B on each side provide adequate surface for fixing.

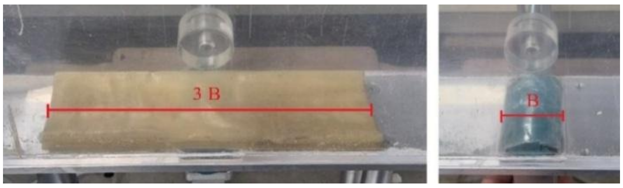

Figure 6. Membrane (left) and half circle (right)

For model preparation, dry tamping methods (Miura & Toki, 1982) were used depending on the target degree of density. The total mass of soil and water required to achieve the desired relative density (D_r) was pre-calculated and was then placed in at least five layers, each approximately 0.02 m thick, and tamped uniformly to reach the target density. This layering approach ensured consistent compaction and minimized density variation throughout the model depth. The trapdoor configuration was fixed at an H/B ratio of 2.5, thus providing a shallow case and a scaled prototype equivalent of a trapdoor 2.4 m wide.

2.3.2 Instrumentation and imaging

To capture soil displacements during trapdoor tests (see Figure 7), Particle Image Velocimetry (PIV) was applied using the GeoPIV8 software (White & Take, 2002). GeoPIV is a MATLAB-based tool that tracks soil surface texture patterns across sequential images to measure displacement fields with sub-pixel accuracy. In practice, the soil surface is divided into a grid of small interrogation patches, and the cross-correlation method is used to determine the displacement of each patch between successive images (see Figure 8). This approach allows accurate visualization of deformation zones and settlement through development in geotechnical model tests. More details on the algorithm, precision, and validation of the software can be found in White and Take (2002). Two reference points, one on the surface and one (2.5 cm) above the trapdoor, were monitored in particular.

Table 1. Tests conducted in study

Test	***Description***	***Trapdoor***	***D_r (%)***	***ρ (kg/m³)***
1	*Dry*	*Tradi-tional*	*90*	*1694.37*
2	*Dry*	*Tradi-tional*	*60*	*1590.64*
3	*Dry*	*Tradi-tional*	*30*	*1498.87*
7	*Dry with mem-brane*	*Mem-brane*	*60*	*1590.64*
8	*Dry with half-cir-cle*	*Half-cir-cle*	*60*	*1590.64*

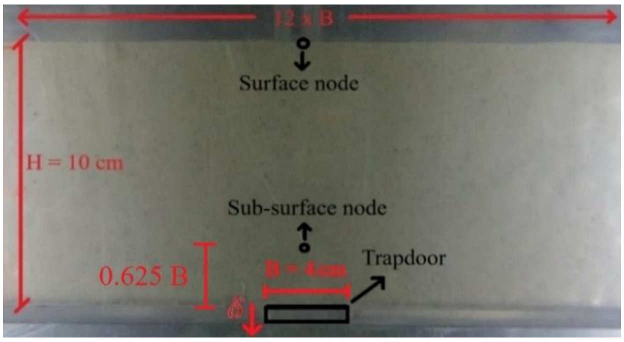

Figure 7. The surface and subsurface node locations

2.4 Numerical trapdoor modeling

To aid interpretation of the experimental trapdoor–soil interactions, a parallel numerical study was conducted using a refined finite element (FE) approach based on prior works (Farasat et al., 2024). The non-linear elastic behavior of the sand was modeled in Abaqus using a combined constitutive framework. The Porous Elastic model was first used to capture nonlinear isotropic elasticity through an exponential pressure–volumetric strain response (Abaqus/CAE 2021).

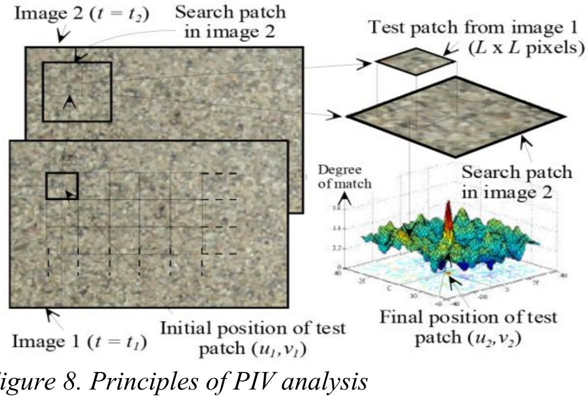

Figure 8. Principles of PIV analysis

To complement this, the Modified Drucker-Prager/Cap Model (MDPC) model was applied to better represent stress–strain behavior, particularly under unloading and reloading. Together, the Porous Elastic and MDPC models provided a realistic description of the sand response across different saturation states. The MDPC model consists of three main yield surfaces as can be seen in Figure 9 (Eskandari & Phillips, 1993). Figure 10 presents the model calibration against experimental triaxial test results, comparing the MDPC (M-C) models, confirming that the selected parameters provide a reasonable fit to the soil stress–strain response.

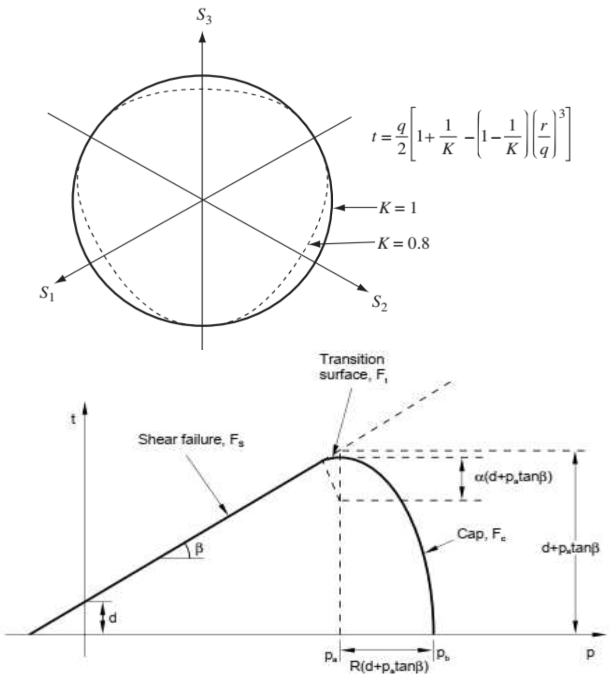

Figure 9. Yield surfaces of the modified cap model in the p–t plane and on the π-plane (Helwany, 2007)

In the numerical simulations, several parameters were held constant across all cases: equivalent friction angle (β = 52.16°), cap eccentricity (R = 0.4), initial yield surface position (ε_{vol}^{in}= 0), transition surface radius (α = 0.25), and flow stress ratio (K = 1) within the MDPC model, along with bulk modulus parameter (κ = 0.0031) and Poisson's ratio (ν′ = 0.3) in the Porous Elastic formulation.

The flexible membrane on the trapdoor in test #7 (see Table 1) was introduced using the Ogden hyperelastic model, chosen for its capacity to capture nonlinear large-strain behavior of elastomeric materials (Farasat et al., 2024). Its strength lies in accurately representing material response regardless of variations in membrane thickness, especially for thinner membranes, where it matches well with experimental results of rubber deflection under fluid pressure (Selvadurai & Shi, 2012). Moreover, the model captures the strain stiffening behavior observed at higher strains (Shahzad et al., 2015), making it highly suitable for membrane simulations where large deformations are expected. Its versatility allows accurate description of material behavior across a range of strains (Selvadurai & Shi, 2012).

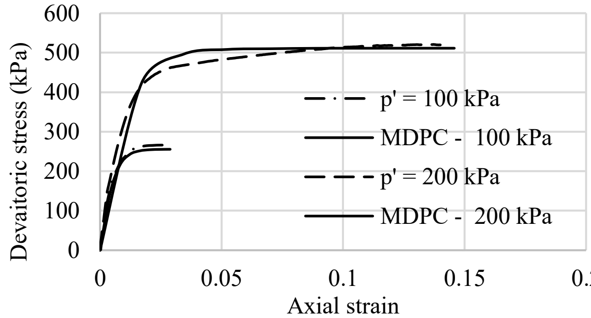

Figure 10. Modified Drucker–Prager/Cap fitting for Barco 32 sand

This model originally introduced by Ogden (1972), the model is based on principal stretches (λ_i). The strain energy function (W) and the initial shear modulus (G_0) are given by the following equations:

$$W = \sum_{i=1}^{N} \frac{2\mu_i}{\alpha_i}\left(\lambda_1^{\alpha_i} + \lambda_2^{\alpha_i} + \lambda_3^{\alpha_i} - 3\right) \quad \text{Eq.2}$$

$$G_0 = \frac{1}{2}\sum_{i=1}^{N} \mu_i \alpha_i \quad \text{Eq.3}$$

λ_i is the deviatoric principal stretch ($\lambda_i = 1 + \varepsilon_i$), ε_i is principal strain, and μ_i and α_i are temperature dependent material parameters. The hyperelastic Ogden model parameters used to simulate the elastomeric membrane response for test #7 of Table 1 are provided in Table 2.

Table 2. Constants for different stiffness rubber materials (Garg, 2023)

Ogden parameters	**Soft – Ecoflex 00-50**
$\mu_1\ (MPa)$	*0.00270414*
α_1	*2.98869*
$\mu_2\ (MPa)$	*0.00270414*
α_2	*2.98869*
$\mu_3\ (MPa)$	*0.00270414*
α_3	*2.98869*
$D_1 - D_3\ (MPa)$	*0*

3 RESULTS

3.1 Modelling overview

Two sets of tests were conducted on active trapdoor models in medium sand under shallow (H/B = 2.5) conditions. Three tests were used with a traditional flat trapdoor to investigate the influence of soil density on surface settlements and subsurface failure mechanisms. A further group of tests were conducted at D_r = 60 % with different trapdoor configurations from flat, to flexible and rigid half-circle. These were anticipated to approximate a flexible system (e.g. culvert) and settlement of a rigid tunnel, respectively.

3.2 Scaled model trapdoor centrifuge results

3.2.1 Effect of density

GeoPIV8 analysis (White & Take, 2002) was performed on images from the tests described in Table 1. Vertical displacements were monitored at surface (N_1) and sub-surface (N_2) nodes (see Figure 7). Responses were evaluated at three normalized trapdoor displacements (δ/B): 0.025, 0.25, and a transition point identified by a sharp increase in the surface displacement slope (see Figure 11 for normalized settlements of tests 1 to 3 and in Figure 13 for surface settlements at Point B).

1. Point A = $\delta_A/B = 0.1/4 = 0.025$
2. Point B = Second downward movement δ_B
3. Point C = $\delta_C/B = 1/4 = 0.25$

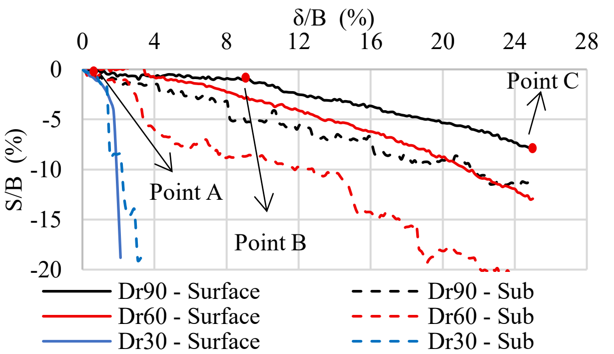

Figure 11. Normalized settlement versus normalized trapdoor settlement for tests 1 to 3

PIV-derived surface (N_1) and subsurface (N_2) displacements for different relative densities (D_r = 30 %, 60 %, 90 %) are shown in Figure 11 highlight the role of soil volumetric behavior during trapdoor deformation. Although these settlement troughs represent different relative movements (δt/B) for the three cases, these are likely to represent the transition to significant arching & displacements and are therefore informative. They also follow the same approach used by (Marto et al., 2015). Dense sand (D_r = 90 %) exhibited greater subsurface than surface displacement at δ = C (4.3 mm vs. 3.24 mm), consistent with a dilative response. Loose sand (D_r = 30 %) showed higher surface displacements (49.26 mm vs. 16 mm), indicating predominantly compressive behavior. The medium-density case (D_r = 60 %) displayed an intermediate but dilation-dominated response, with larger subsurface movement (8.1 mm vs. 5.16 mm), reflecting volumetric expansion below the surface.

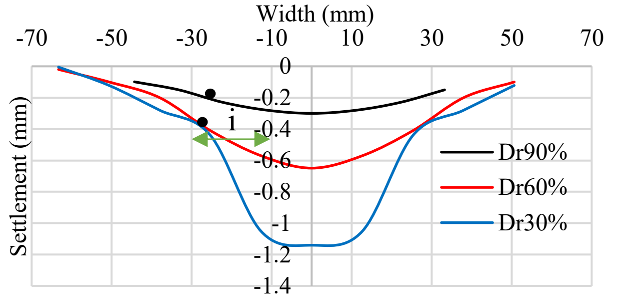

Figure 12. Experimental surface settlement for different relative density at the second displacement point (B)

Surface settlement trough shape shown in Figure 12 shows that it also varies with density. Loose sand (D_r = 30 %) exhibits a wider and deeper trough, indicating a broader influence zone, while dense (D_r = 90 %) shows a flatter, more localized profile due to stiffer, dilative deformation. These trends are consistent with critical state soil mechanics and highlight the role of density in surface response. The inflection points shift outward with decreasing density (x = 25 mm for D_r = 90 % and x = 30 mm for D_r = 60 % and 30 %), indicating weaker arching and wider deformation in looser sand.

3.2.2 Effect of Trapdoor Geometry and Boundary Flexibility

This group comprises of Tests 7/8, designed to investigate how the trapdoor geometry and boundary flexibility influence soil arching behavior. Test 7 employed a flexible latex membrane (length of 12 cm and thickness of 3 mm) to represent a deformable tunnel boundary, while Test 8 used a rigid half-circle trapdoor (the diameter of 4 cm) simulating a circular tunnel profile. Comparing these two cases with the traditional flat rigid trapdoor (4 cm) highlights the role of structural flexibility and curvature in stress redistribution, deformation localization, and the efficiency of arch formation within the soil mass.

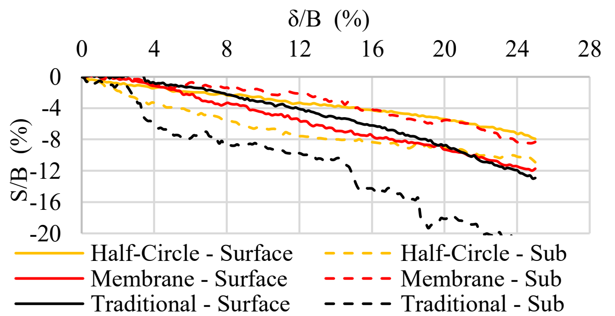

Figure 13. Normalized settlement versus normalized trapdoor settlement of tests 1, 7 and 8

Figure 13 presents the normalized surface and subsurface settlement responses (S/B) as a function of normalized trapdoor displacement (δ/B) for the rigid trapdoor, membrane and half-circular configurations. Settlement increases with increasing trapdoor displacement in all cases. At early stages of displacement, the half-circle trapdoor shows slightly deeper settlements than the membrane; however, at larger displacements the half-circle response becomes shallower, reflecting the development of stronger localized arching. This indicates that both boundary flexibility and curved geometry reduce settlement magnitudes compared to the traditional configuration.

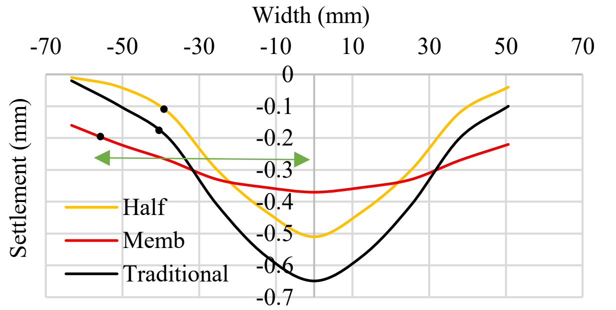

Figure 14. Experimental surface settlement for different tunnel lining flexibility of D_r = 60% at the second point (B)

Figure 14 demonstrates that tunnel lining stiffness strongly controls surface and subsurface settlement behavior at D_r = 60 % at point B. The flexible membrane produces the smallest settlements, characterized by a shallow and wide trough, due to its ability to deform with the soil, provide tensile resistance, and redistribute stress laterally. The rigid half-circle shape results in greater settlement than the membrane, but less than the unsupported reference case, forming a narrower and deeper trough as stresses are redirected into the surrounding soil. The reference D_r = 60 % flat case exhibits the largest settlements, reflecting unrestricted soil deformation. At large trapdoor displacements, both membrane and half-circle cases reduce settlements compared to the baseline, with the membrane being the most effective. The inflection point analyses shows that the membrane significantly widens the zone of influence, while rigid and half-circle configurations localize deformation, highlighting the combined effects of lining stiffness and geometry on soil arching.

Figure 15 shows vertical settlement contours and displacement vectors at Point C for the traditional, membrane, and half-circle trapdoor configurations, highlighting the influence of geometry and boundary flexibility on deformation behavior. The traditional trapdoor exhibits a concentrated zone of large vertical settlements with predominantly downward displacement vectors, indicating weak arching and limited lateral load transfer. The membrane trapdoor produces a broader and shallower settlement trough with more distributed displacement vectors, reflecting gradual stress redistribution and reduced strain localization. In contrast, the half-circle trapdoor shows reduced peak settlement with more pronounced lateral displacement toward the sides, indicating the development of a localized arching mechanism promoted by the rigid curved geometry.

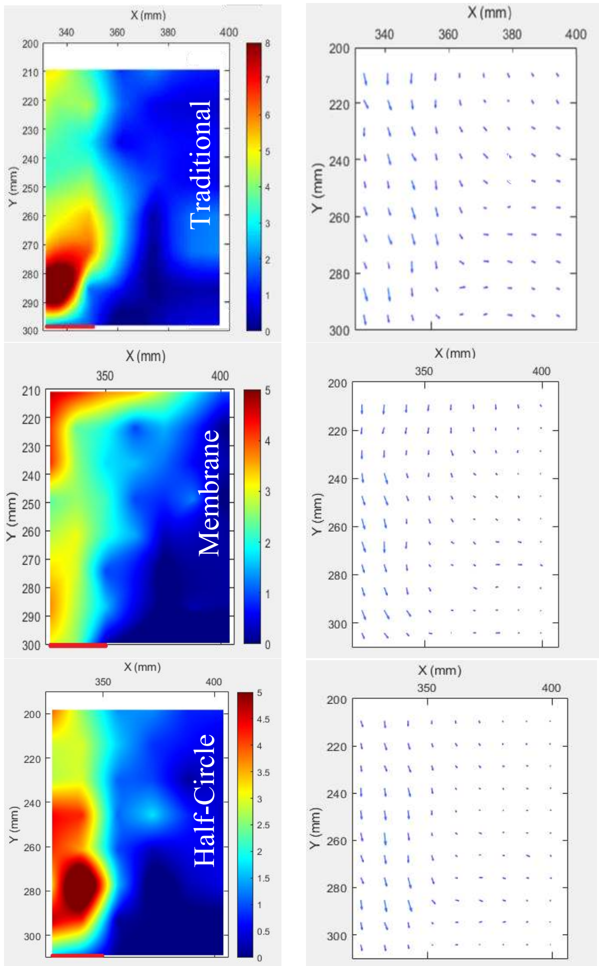

Figure 15. Vertical settlement for different trapdoor setups at point C

3.3 Interpretation with numerical modelling

A series of supporting finite element analyses were performed to aid test interpretation and limited data is shown herein; additional predictions are available in Farasat (2026). In Figure 16, the volumetric strain response differs markedly between the half-circle and membrane trapdoors at D_r = 60 %. The half-circle trapdoor shows negligible volume change at small displacement, but clear localized dilation develops along the curved edges as displacement increases, indicating concentrated arching and shear-induced expansion of the dense sand. In contrast, the membrane trapdoor exhibits weaker and more distributed volumetric strain, with dilation developing gradually and remaining lower in magnitude even at large displacement. Overall, the half-circle promotes localized dilative volumetric strain, while the membrane leads to milder, spatially distributed volume change. These volumetric localizations are also accompanied by principal stress rotations and show the development of arching.

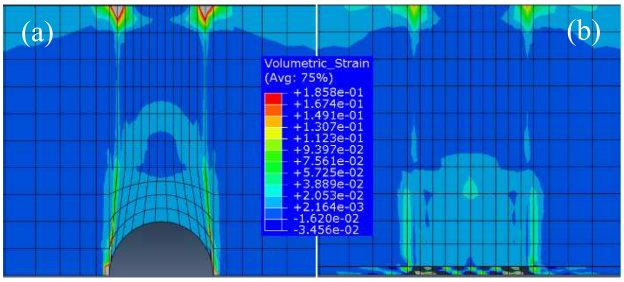

Figure 16. Shear strain for trapdoor movement of δ/B = 0.125 for D_r=60% with the membrane and half-circle

Figure 17 presents the vertical (AB and CD) and horizontal (EF) stress paths used to assess arching behavior around the trapdoor for the flat, half-circle, and membrane configurations. Figures 18 and 19 illustrate vertical stress redistribution along the trapdoor centerline (CD) and across the trapdoor span (EF) for different boundary configurations at Dr = 60%. Along line CD, vertical stress profiles at small displacement (δ/B = 0.025) are similar for all cases, indicating limited stress relief above the trapdoor. At larger displacement (δ/B = 0.125), the traditional trapdoor shows pronounced reduction in vertical stress above the opening, reflecting inefficient arching. In contrast, the half-circle retains higher stress along the centerline, consistent with effective arch formation, while the membrane shows intermediate stress reduction due to load sharing.

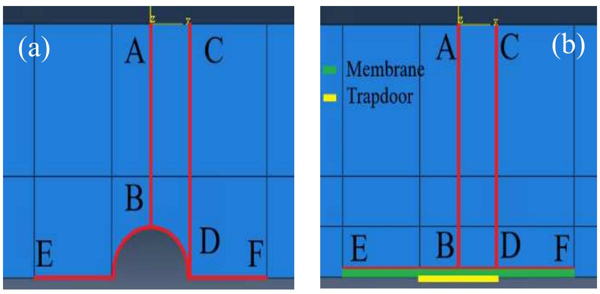

Figure 17. Vertical (AB and CD) and horizontal (EF) stress paths for a) Half-circle and b) membrane

Along line EF, little lateral stress redistribution is observed at small displacement. At δ/B = 0.125, however, the half-circle trapdoor develops clear stress concentrations near the trapdoor edges with reduced stress at the center, indicating strong lateral load transfer. The traditional trapdoor shows sharper stress gradients and localized stress drops, while the membrane displays a more distributed stress profile.

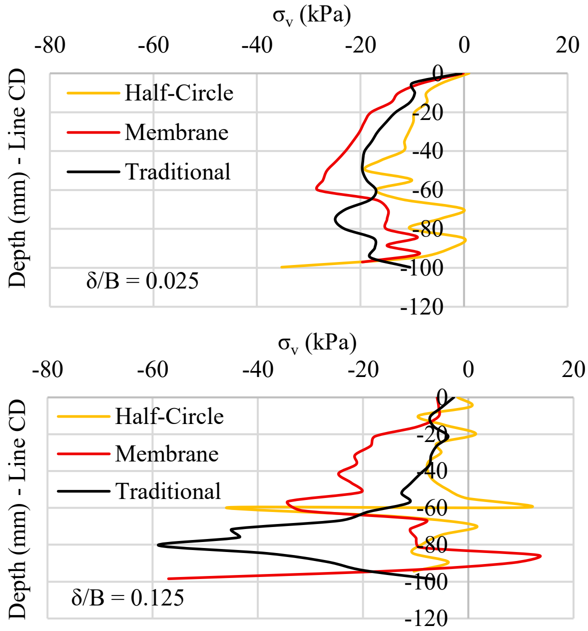

Figure 18. Vertical stress at trapdoor edge line (CD)

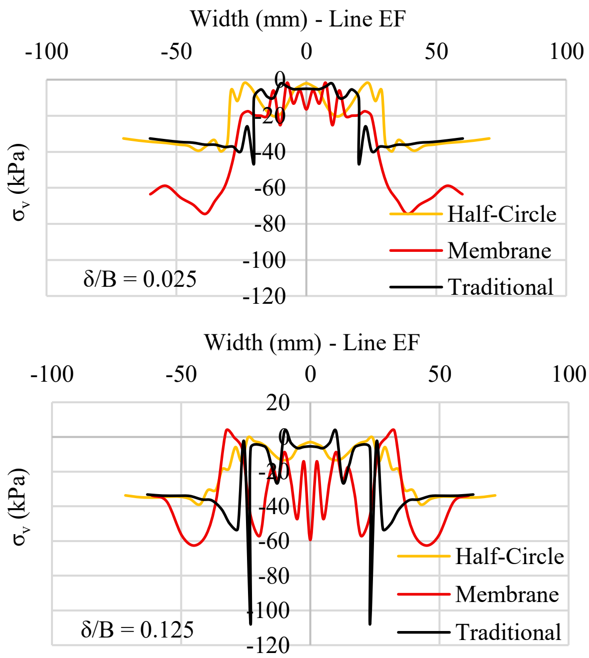

Figure 19. Vertical stress along the trapdoor (EF)

4 CONCLUSION

This study investigated effects of soil relative density, trapdoor geometry and flexibility on arching mechanisms and ground deformation in dry sands for active trapdoors. The results show that changes in soil state and trapdoor configuration produce distinct differences in settlement response, strain patterns, and stress redistribution.

- Soil relative density strongly governs arching behavior. Loose sand exhibited weak arching, large settlements, and diffuse shear strain, indicating a collapse response. Medium-dense sand showed partial arch formation with moderate settlements and strain localization. Dense sand mobilized the most arching, characterized by localized strain near trapdoor edges and minimal settlement.

- Trapdoor geometry also significantly influences load redistribution. The half-circle trapdoor produced the most efficient arching, with symmetric strain localization and stress transfer to surrounding soil, resulting in a narrow deformation zone.
- The half-circle trapdoor induces localized dilation associated with concentrated arching and the membrane exhibits weaker/more distributed volumetric strain, indicating milder arching response.
- At large displacement, the half-circle configuration retains higher stress above the opening and transfers load to the sides, the traditional trapdoor shows significant stress reduction, and the membrane exhibits more gradual redistribution.

5 REFERENCE

Abaqus/CAE User's Manual. (2021). Abaqus 6.11 Abaqus/CAE User's Manual. In Abaqus 6.13 documentation Dassault Systemes Simulica.

Al-Naddaf, M., & Han, J. (2021). Spring-Based Trapdoor Tests Investigating Soil Arching Stability in Embankment Fill under Localized Surface Loading. J. of Geotech and Geoenv Eng., 147(9), 1–11.

Bosscher, P. J., & Gray, D. H. (1986). Soil Arching in Sandy Slopes. J. of Geo Eng., 112(6), 626–645.

Costa, Y. D., Zornberg, J. G., Bueno, B. S., & Costa, C. L. (2009). Failure Mechanisms in Sand over a Deep Active Trapdoor. J. of Geotech and Geoenv Eng., 135(11), 1741–1753.

Deljoui, P. (2012). Upheaval buckling of offshore pipelines in homogeneous and layered soils (PhD thesis). Western University, London, Canada.

Eskandari, F., & Phillips, R. (1993). A state parameter modified Drucker–Prager cap model. Proc 46th Canadian Geotech. Conf., 288–295.

Farasat, N. (2026). Tunnelling in soft saturated granular soils. Western University (PhD thesis). Western University, London, Canada.

Farasat, N., Newson, T., & Boone, S. (2024). The effect of membrane flexibility on the behavior of 2D-tunnel excavation models in granular soils. Proceedings of the 17th Pan-American Conf. on Soil Mechanics and Geotech. Eng. 1-8.

Garg, H. (2023). Mechanical testing of synthetic biomaterials for organ simulation (Master's thesis). Texas Tech University, Lubbock, Texas.

George, T. I., & Dasaka, S. M. (2021). Numerical Investigation of Soil Arching in Dense Sand. Int. J. of Geomechanics, 21(5)(August).

George, T. I., & Dasaka, S. M. (2023). Mechanics of arch action in soil arching. Acta Geotechnica, 18(4), 1991–2009.

Handy, R. L. (1985). The Arch in Soil Arching. J. of Geotech. Eng., 111(3), 302–318.

Helwany, S. (2007). Applied Soil Mechanics with ABAQUS Applications. John Wiley & Sons.

Ladanyi, B., & Hoyaux, B. (1969). A study of the trapdoor problem in a granular mass. Canadian Geotech. J., 6(1), 1–14.

Marto, A., Abdullah, M. H., Makhtar, A. M., Sohaei, H., & Tan, C. S. (2015). Surface settlement induced by tunneling in greenfield condition through physical modelling. Jurnal Teknologi, 76(2), 1–7.

McNulty, J. (1965). An experimental study of arching in sand (PhD thesis). University of Illinois.

Miura, S., & Toki, S. (1982). Sample Preparation Method and Its Effect on Static and Cyclic Deformation - Strength Properties of Sand. Soils and Foundations, 22(1), 61–77.

Osman, A. S., Jacobsz, S. W., & Purchase, C. (2019). Numerical analysis of cavity propagation in deep trapdoor experiments. Proceedings of the XVII ECSMGE-2019. 1-7.

Rai, H., & Chavda, J. T. (2023). Evaluation of Drained Stability of Active and Passive Trapdoors for Horizontal and Inclined Soil Bed using Finite. Transportation Infrastructure Geotechnology.

Selvadurai, A. P. S., & Shi, M. (2012). Fluid pressure loading of a hyperelastic membrane. Int. J. of Non-Linear Mechanics, 47(2), 228–239.

Shahzad, M., Kamran, A., Siddiqui, M. Z., & Farhan, M. (2015). Mechanical characterization and FE modelling of a hyperelastic material. Materials Research, 18(5), 918–924.

Terzaghi, K. (1943). Theoretical Soil Mechanics. In John Wiley & Sons.

Wagle, G. S., Engel, R. S., Bollina, R., & German, R. M. (2003). Statistical Analysis of Modified Drucker-Prager Cap Model Parameters for Application to Modeling Die Compaction. ResearchGate, 24–36.

Wang, W., & Yen, B. C. (1974). Soil arching in slopes. J. of the Geotech. Eng. Division, ASCE, 100(GT1), 61–78.

White, D. J., & Take, W. A. (2002). GeoPIV: Particle image velocimetry (PIV) software for use in Geotech. testing (Technical report). University of Cambridge.